Effects of Through-Thickness Fiber Geometry and Small Angle on Impact Resistance

G.C. Coppens and D. Liu
Dept. of Mechanical Engineering, Michigan State University, East Lansing, MI
E-Mail: liu@egr.msu.edu

Abstract

This paper compared the impact resistance of laminated, stitched, two-dimensional woven and innovative three-dimensional woven composite plates. All composite plates were made from the same glass/epoxy prepreg tape so direct comparisons could be made about the effects of through-thickness fiber geometry on impact resistance. The effects of small fiber angles between adjacent composite layers were also studied. The laminated plates had no additional through-thickness reinforcement while the stitched plates were reinforced through the thickness with one-millimeter wide strips of prepreg. The two-dimensional and three-dimensional woven plates were hand made using 12.7 mm wide strips of prepreg. The three-dimensional weaving technique incorporated innovative fabric geometry to reinforce the plates through the thickness. The stitched plates were found to have the highest impact resistance followed by the three-dimensional woven plates. The laminated plates had the lowest impact resistance. The laminated and three-dimensional woven plates with smaller fiber angles between adjacent layers also had higher impact resistance than those with larger angles. Through-thickness geometry and small fiber angle seemed to increase delamination resistance and impact resistance.

Introduction

Composite materials offer high strength-to-weight and stiffness-to-weight ratios making them excellent candidates for use in structures where strength must be maximized while minimizing weight such as high-performance airplanes and cars. Composites can also be used as armor for civilian and vehicle applications due to their high energy absorption capabilities. Their role is to provide penetration resistance, impact energy dissipation, and damage containment[1]. Material selection of fibers and matrix, stacking sequence, and translaminar reinforcing techniques are some of the factors taken into account when designing composite armor.

Although composite materials offer many benefits when compared to conventional metals, they are susceptible to transverse loading. One of the weaknesses of composites is their tendency to delaminate when loaded transversely. Delamination can cause severe reductions in strength and stiffness, which can lead to failure of an entire structure. This drawback may be one of the limiting factors on composite materials being used in more areas[2]. Other forms of damage associated with transverse loading include matrix cracking, fiber-matrix debonding, fiber microbuckling, fiber shear-out, and fiber fracture[3,4].

The amount of energy that composites can resist before penetration and perforation is reduced by delamination[5]. Transverse damage resistance is especially poor in laminated composites because they have no through-thickness reinforcement. There have been many studies on laminated composites subjected to low-velocity impact as evidenced by the review of Richardson and Wisheart[6]. Most studies agree that the most detrimental damage in composite laminates subjected to impact loading is delamination[2,7]. This type of damage can occur by relatively light impacts while the surface appears to be undamaged[8]. Laminated panels are still attractive because there are no crimp angles which can reduce the in-plane properties and fiber volume fractions.

Many methods have been investigated with the goal of increasing the interlaminar fracture toughness of laminated composites. These include using toughened thermosetting matrices, translaminar reinforcement in the form of stitching, z-pinning, knitting, braiding, weaving, and modifying interfacial properties. Some studies have shown stitching can increase compression after impact strengths by 50% and increase Mode I fracture toughness by a factor of 30[9]. Larsson found that stitching could increase impact delamination energy by more than 20 times when compared to unstitched plates[10]. This is because the stitching improves the delamination resistance energy by raising the Mode I interlaminar fracture resistance of the laminate, which makes it more difficult for a delamination crack to propagate between the fiber layers[11]. Stitching clearly has many benefits. However, there are problems associated with stitched composites. These include difficulties in stitching complex shapes along with size and thickness restraints imposed by the sewing machines. Large purpose-built sewing machines require extremely high capital costs[12]. Stitching can also decrease in-plane stiffness and tensile and compressive properties by varying amounts[13]. The thread and needle used for stitching can damage the microstructure by breaking, spreading, and crimping the fibers around the stitch holes. Resin rich regions form around the stitch holes causing possible stress concentration zones[11].

Composite plates made from two-dimensional woven fabric have received much attention. Two-dimensional fabric consists of plain, satin, twill, etc. weaving geometries. Two-

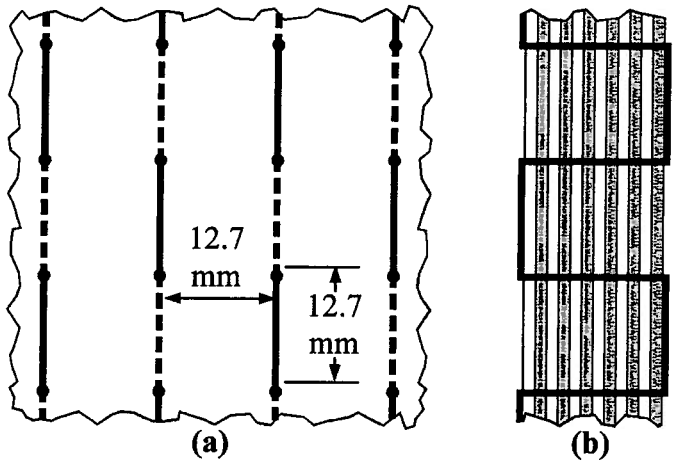

Figure 1. Stitching pattern (a) top view and (b) cross section.

dimensional fabrics offer improved impact resistance and damage tolerance because of their integrated nature and balanced in-plane properties[14]. Woven fabric laminates have been shown to have Mode I interlaminar fracture toughness of four to five times greater than laminates made of unidirectional fabric. This can be attributed to the roughness of the fabric, resin rich regions between the layers, and the ways in which crack propagation occurs[2]. The resin rich areas tend to arrest the interply cracks and cause them to "jump" between undulations rather than extend continuously. The cracks also have difficulty in propagating because of the undulating paths that occur in the fabric[15]. Woven fabrics also have smaller damage areas after impact, thus they have higher residual compression strength when compared to unidirectional laminates. These strengths can be attributed to the more ductile and compliant nature of woven fabrics[2]. Siow and Shim studied plain weave carbon epoxy plates with a quasi-isotropic laminate. They found the damage mechanisms for woven laminates to be mainly delamination and fiber breakage which were similar to unidirectional laminates[16].

Three-dimensional composites have become very popular based on their greater delamination resistance, ballistic damage resistance and impact damage tolerance. Weaving, braiding, stitching, and knitting are all methods for producing three-dimensional composites. The impact energy needed to initiate damage in three-dimensional carbon-bismaleimide composites is up to 60% higher than in a laminated counterpart of the same materials. Their Mode I interlaminar fracture toughness values can be 6-20 times higher than unidirectional composites. This group of composites gets their superior properties from the through-thickness binder yarns which can arrest or slow the growth of delamination cracks[12]. However, many of the in-plane properties of three-dimensional composites are inferior to laminated counterparts when an equivalent amount of fibers are aligned in the load direction. Their stiffness values are similar to two-dimensional woven fabrics but their tension and compression strengths may be lower by 15-20%. The strength reduction is due to the crimping and distortion of in-plane fibers by the binder yarns[12].

This study attempted to raise the energy level required to cause penetration and perforation of glass/epoxy composite plates. There are two primary ways to achieve this goal; one is to use through-thickness stitching and the other is to use woven fabrics. The use of identical composite constituents allowed direct correlations to be made between microstructure parameters and impact resistance.

Fabrication

All composite plates constructed for this study were made from Scotchply type 1003-A tape which was a non-woven, unidirectional fiberglass tape pre-impregnated (prepreg) with an epoxy matrix. The prepreg tape came on a 300 mm (12") wide roll with a total length of 66 m (72 yards).

Laminated Plates

Laminated composite plates were constructed from twelve pieces of prepreg tape. Each piece was 300 mm x 300 mm. The angled plies were cut by using patterns. The plates had an unsymmetric stacking sequence of [0/θ/0/θ/0/θ/0/θ/0/θ/0/θ] with θ being equal to 7.5, 15, 30, 45, or 90 degrees. They were designated as $L[(0/\theta)_6]$.

Stitched Plates

The stitched plates were based on a laminated stacking sequence of $L[(0/90)_6]$ which was also unsymmetric. The stitching was done by hand using a needle and 1 mm wide strips of prepreg for thread. A horizontal stitching pattern was used as shown in Figure 1a. The nodes in the figure represent the stitching points for a portion of a plate. The solid and dashed lines represent the threads above and below the plate, respectively. The path of the thread through the plate is shown in Figure 1b. The distance between each stitch as well as each row of stitching was 12.7 mm forming unit cells of 12.7 mm x 12.7 mm. The stitched plate was designated as $S[(0/90)_6]$.

Two-Dimensional Woven Plates

The two-dimensional (2D) woven plates consisted of six pieces of plain weave prepreg that were stacked together. Each piece was very similar to a layer of conventional woven fabric composite. However, each piece was manufactured from interweaving 12.7 mm wide strips of prepreg in the warp and fill directions rather than from a prefabricated woven fabric. Each piece was woven by hand using a fabricated loom. The six pieces were then stacked together with both warp and fill units well aligned through the thickness. The 2D woven plates with the geometry shown in Figure 2 were designated as $2D[(\underline{0/90})_6]$, where the underline emphasized woven. The panels had dimensions of 300 mm x 300 mm after removing the excessive warp and fill units from all edges. Though not exact, the 2D woven composite plate was close to being symmetric about its midplane.

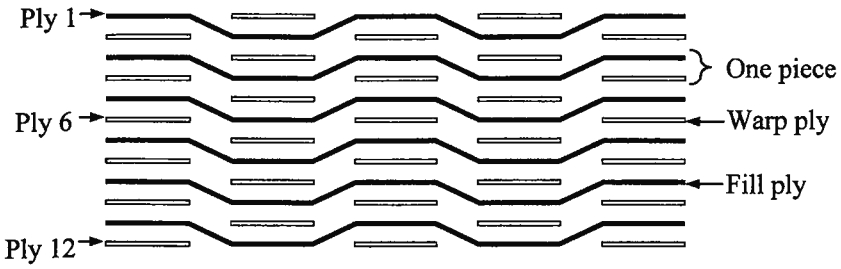

Figure 2. Side view of 2D woven geometry.

Three-Dimensional Woven Plates

The three-dimensional (3D) woven plates used a novel manufacturing technique [x] to create a geometry in which 12.7 mm wide strips of prepreg were interwoven in the warp, fill, and through-thickness directions. The geometry of the 3D woven plates was similar to that of the 2D woven plates; however, each piece of the 3D woven plates was interwoven with the neighboring pieces in the thickness direction. On the contrary, the 2D woven plates consisted of six pieces of plain-woven prepreg that were joined by the epoxy matrix between them. Figure 2 shows that in a 2D woven plate, plies 1 and 2, 3 and 4, 5 and 6, 7 and 8, 9 and 10, and 11 and 12 were woven together. The 3D woven plate differs because in the warp direction plies 1 and 2, 2 and 4, 4 and 6, 6 and 8, 8 and 10, and 10 and 12 were interwoven together as shown in Figure 3a. Plies 1 and 3, 3 and 5, 5 and 7, 7 and 9, 9 and 11, and 11 and 12 were interwoven in the fill direction as shown in Figure 3b. This three-dimensional geometry created plates with the same thickness as the 2D woven plates with fibers connecting the neighboring pieces.

The 3D woven plates had orthogonal as well as non-orthogonal angles between warp and fill strips. The fill strips were placed at angles of 15, 30, 45, and 90 degrees from the warp strip direction. These plates were designated as 3D[(0/15)$_6$], 3D[(0/30)$_6$], 3D[(0/45)$_6$], and 3D[(0/90)$_6$]. The plates had dimensions of 300 mm x 300 mm after the edges were trimmed.

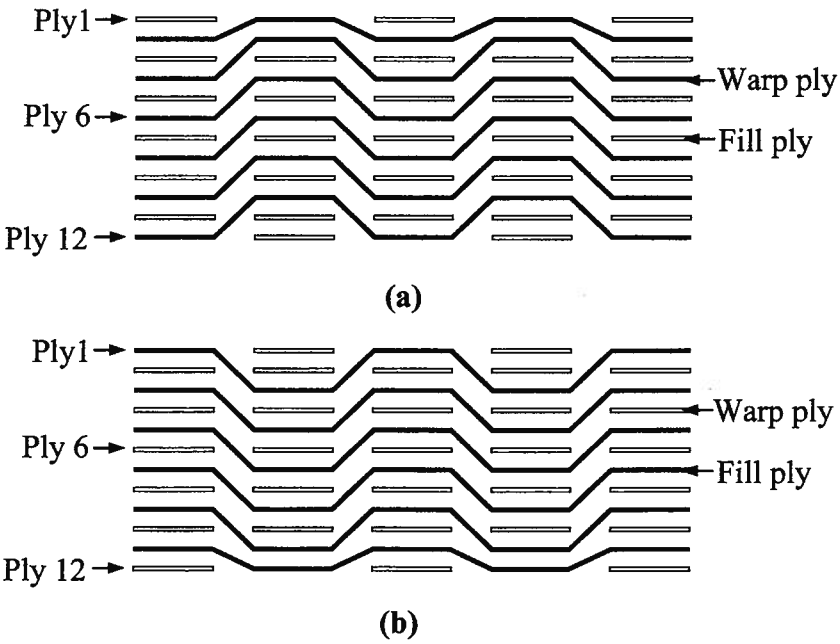

Figure 3. Three-dimensional weave geometry in warp and fill directions.

Curing

The composite plates were cured in an autoclave. Six panels were cured at a time to ensure that they all received the same cure cycle. The cure cycle included (1) setting pressure in autoclave to 560 kPa, (2) ramping temperature from room temperature to 160°C at 10° per minute, (3) holding temperature at 160°C and pressure at 560 kPa for 45 minutes and (4) cooling from 160°C to room temperature at 10° per minute then releasing pressure. Only one caul plate was used, i.e. the vacuum bag was not sandwiched between two caul plates as in conventional autoclave procedures. This allowed composite plates freedom to warp which was caused by their unsymmetric stacking sequences.

All of the composite plates warped slightly. The laminated and stitched specimens had thickness around 2.6 mm. The woven specimens were approximately 0.1 mm thicker, i.e. 2.7 mm, because of the resin pockets due to the fabric geometries.

Testing

Impact Testing Machine

The composite plates were tested with an instrumented drop-weight impact tester. Each 300 mm x 300 mm plate was cut into nine 100 mm x 100 mm specimens with a diamond blade circular saw. The drop weight tester consisted of the items labeled in Figure 4. The 12.7 mm diameter tup with a hemispheric nose was connected to a 22,241 N load cell that was attached to the crosshead. The tup had an overall length of 50.8 mm and a mass of 92.4 g. The total weight of the crosshead, load cell, and tup was 49.3 N, which corresponded to a mass of 5.03 kg.

The rebound arrestor consisted of a pneumatic air cylinder, a solenoid valve, relay, a toggle switch, and a roller lever switch. The switches were held in place by a stand. The top and bottom plates of the specimen clamping fixture had cutouts of 76 mm x 76 mm. Four toggle clamps were used to secure the top plate and the specimen to the bottom plate. Toggle clamps were used to ensure that the clamping points and clamping forces were consistent for all types of specimens tested. Clamping resulted in a fixed boundary condition simulating that the specimens were small sections of large structures.

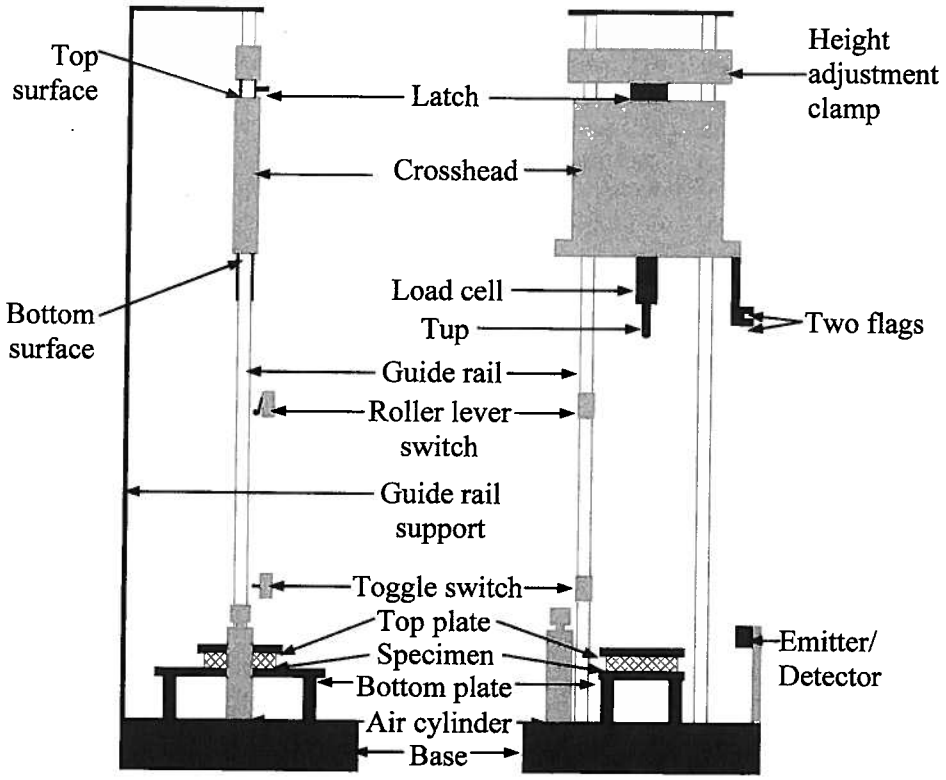

Figure 4. Schematic diagram of impact testing machine.

Testing Procedures

Each test consisted of placing a 100 mm x 100 mm specimen on the bottom plate of the clamping fixture. The top plate was then placed over the specimen and secured with the toggle clamps. The crosshead was then raised to a desired height above the specimen by adjusting the position of the height adjustment clamp. Finally, the latch was pressed to release the crosshead. The crosshead would drop under the force of gravity and be guided by the rails. The tup would strike the specimens at their centers. The centers of the stitched and woven composites were carefully adjusted to be the centers of their unit cells. This resulted in the best condition for impact.

A photogate system consisting of the two flags and an infrared emitter/detector was used to determine the impact velocity v_i. The signal normally read by the computer was zero volts. The flags, shown in Figure 4, would produce two five-volt spikes in the signal as they passed through the emitter/detector. Each flag would produce its own individual spike. The data acquisition software would then measure the time between the two spikes. This time, t, and the distance, d (10.3 mm), between the two flags could be used to determine the impact velocity, i.e. $v_i = d/t$. Both flags needed to be just below the emitter/detector when the tup made contact with the specimens for the computer to be triggered correctly.

The crosshead would move past the roller lever switch then the bottom surface of the crosshead would move the toggle switch to the "on" position while dropping by striking the toggle. This would cause power to be sent to the roller lever switch. In the event of the tup rebounding, the roller lever switch would be hit by the top surface of the crosshead. Since the roller lever switch would have power when the crosshead hit it the second time, the relay would latch and open the solenoid valve causing the air cylinder to extend thus preventing the tup from hitting the specimen a second time. The toggle switch was positioned so that it would be turned "on" just as the tup made contact with the specimens. The roller lever switch was located 270 mm above the toggle switch for all tests. The load on the tup during impact was recorded by a computer and subsequent data analysis was performed by a computer program.

Testing Measurements

The composite specimens were tested by adjusting the drop height while keeping the crosshead weight constant. Tup load, F(t), was recorded at a sampling rate of 25 μs which was used to calculate the acceleration, a(t), after dividing by the combined mass, m, of the crosshead, load cell, and tup, i.e.

$$a(t) = F(t)/m \qquad [1]$$

Throughout this study, m was equal to 5.03 kg for all tests. The computer would record 2048 data points during each test resulting in the maximum capability of recording an impact event of 50 ms. This duration was sufficient for all of the impact tests performed in this study. The velocity, v(t), at each time step was calculated by integrating the acceleration, a(t), using Equation 2 where 0 corresponded to the time when the computer began recording load data, t was the duration of the event, and v_i was the impact velocity measured by the photogate system.

$$v(t) = -\int_0^t a(t)dt + v_i \qquad [2]$$

The deflection history, δ(t), was caluculated by integrating the velocity history using Equation 3.

$$\delta(t) = \int_0^t v(t)dt \qquad [3]$$

Since both load and deflection could be expressed as functions of time, the direct relation between load and deflection, i.e. the load deflection relation

$$F = f(\delta) \qquad [4]$$

could be established. The load-deflection curve was then used to determine the absorbed energy, E_a, using Equation 5 where δ_t was the deflection when the force became zero again at the end of impact.

$$E_a = \int_0^{\delta_t} F(\delta)d\delta \qquad [5]$$

The tup was made of high carbon steel and subjected to heat treatment. It was assumed to be perfectly rigid for all tests conducted. The load applied to the tup was transferred to the load cell that would deform and the deformation would be measured by the attached strain gages. The strain measurement would then be multiplied by a calibration factor to calculate the load. The assumption of perfect rigidity and the mass (92.4 g) of the tup in front of the load cell, along with the accuracy of the calibration factor, could cause some errors to the measurement of the tup load, F(t).

Data Analysis

Energy Description

The objective of this study was to determine the energy levels required to cause penetration and perforation of composite plates, the so-called impact resistance. A method based on comparing impact energy E_i and absorbed energy E_a was used for determining the thresholds[17]. The impact energy values included both kinetic energy and potential energy. The absorbed energy values assumed all forms of energy absorption, such as elastic and plastic deformation, fracture, and friction. There was also energy absorbed by the testing facility in terms of vibration. Hence, the absorbed energy values were usually less than their respective impact energies for specimens subjected to transverse impact.

As the crosshead is raised, both the impact energy and the absorbed energy increase. There is a point where the impact energy and the absorbed energy first become closest to each other. This point is called the penetration point and the corresponding energy value, the penetration threshold. As the impact energy further increases, the impact and the absorbed energies remain close to each other, namely, the penetration process zone. There comes another point just before the impact energy becomes greater than the absorbed energy again. This point is called the perforation point and the corresponding energy value, the perforation threshold.

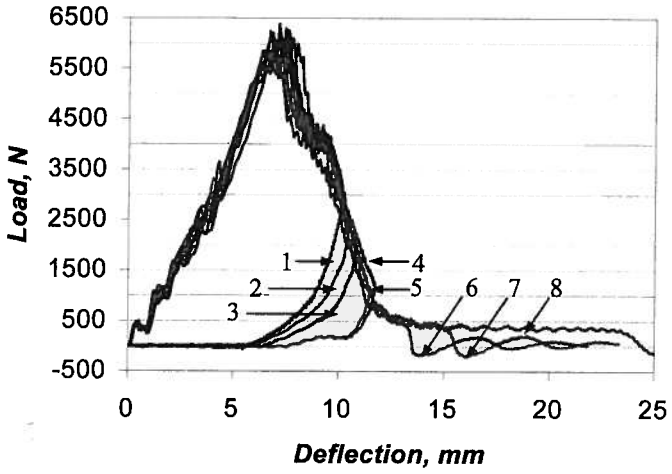

Figure 5. Load-deflection curves of L[(0/90)$_6$] specimens.

Load-deflection Curves

The tup first impacted the specimens with its hemispheric nose. The recording of the load data was started by the flag passing through the emitter/detector. The load data was recorded continually as the tup advanced into the specimens. The recording of the load data was terminated when the load became zero or slightly negative. The load value was not zero when perforation took place for the specimens tested. This was attributed to the sides of the tup rubbing on the specimens and the induced shear loads developing into normal loads at the load cell. Since the data recording unit did not know when the tup perforated the specimens, it kept recording load data even when the load was caused by the sides of the tup rubbing on the specimens. This caused the time of the impact event to be much longer than it took the tup to perforate the specimens. Consequently, the area under the load-deflection curves was increased. When the load was integrated with respect to deflection, excessive absorbed energies were calculated which did not correctly portray the behavior of the impacted specimens. The specimens would seem more resistant to perforation than what they really were. The excessive recording of load data and the friction slippage beyond the penetration point required special attention in the data analysis.

Figure 5 shows eight load-deflection curves of the L[(0/90)$_6$] specimens. They all have a mountain-like shape indicating a significant strain softening after the peak force. The loading sections are slightly concave due to the in-plane constraint caused by the fixed boundary condition. The eight loading sections seem to overlap up to some extent and the values of the eight peak forces are very similar. The unloading sections also overlap well. The overlapping and similarities of the curves indicate the consistency of material properties and testing conditions among the eight specimens. Rebounding resulted in closed curves while penetration and perforation produced open curves. The curves of specimens 1-5 have rebounding sections while the remaining curves do not.

Determination of Energies

Absorbed energies for the specimens with rebounding sections were determined by calculating the areas enclosed by the load-deflection curves. Absorbed energies for the specimens with open curves, such as specimens 6-8, were determined by calculating the area bounded by the load-

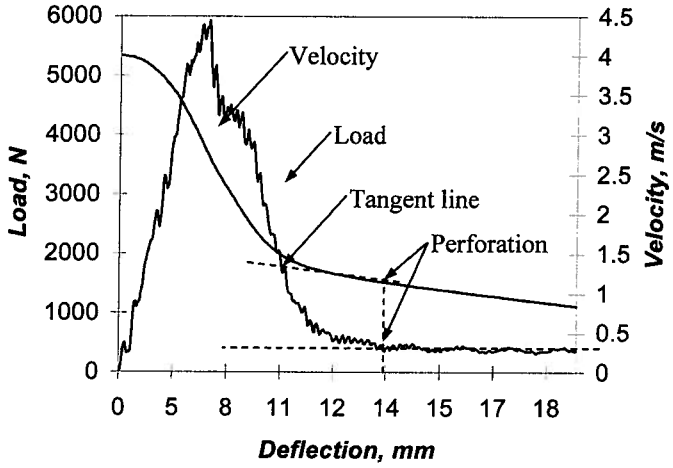

Figure 6. Load and velocity curves of L[(0/90)$_6$] specimen 8.

deflection curves and the horizontal axis, i.e. the deflection axis. The long tail of the open curves indicated an additional absorbed energy from friction between the sides of the tup and the specimens. This friction occurred after the tup perforated the specimens. It maintained a relatively constant energy absorption level.

A. Absorbed Energies

The goal of the drop weight testing was to determine the amount of the energy that each specimen could absorb up to perforation. The calculation of absorbed energies would be correct if the load-deflection curves ended at the perforation points, instead of at the ends of the impact events. A method based on velocity-deflection curve was developed to determine the absorbed energies. This method was useful for the specimens with open load-deflection curves. However, this method did not apply to the specimens with closed load-deflection curves because there was no friction between the tup and the specimens due to the rebounding process.

The corresponding velocity-deflection curve was used to determine the perforation point. The reason was that the velocity-deflection curves leveled off once perforation occurred due to the steady process of friction, i.e. no further damage process in the composite plates. Figure 6 presents the load-deflection curve and the corresponding velocity-deflection curve of L[(0/90)$_6$] specimen 8.

The load value in Figure 6 increased quickly, reached a peak value of 5923 N, and then decreased sharply. The load value then leveled off and became nearly a constant value of 400 N. Friction between the sides of the tup and the specimen started when the load became nearly constant. The point where the load became constant was deemed the perforation point.

The velocity-deflection curve began with a value of 4 m/s which corresponded to the impact velocity. The velocity decreased as the tup was in contact with the specimen. There was then a bend in the curve as the load approached the peak value and then the velocity decreased at a constant rate along the unloading section of the load-deflection curve. Another bend occurred in the velocity near the end of unloading. The velocity decreased constantly again after that point. The starting point of the second constant decrease in velocity was indicative of the starting point of constant friction between the sides of the tup and the specimen. Thus, the constant decrease in velocity began when the tup perforated the specimens. A tangent line with respect to the velocity-deflection curve was drawn to identify the perforation point as shown in Figure 6. Another fitting line was drawn on the load-deflection curve, also shown in Figure 6. The perforation points determined by the load and velocity curves agreed were very close.

This method of determining the perforation points was similar to that used by Baucom and Zikry[18]. In their study, the specimens were deemed perforated when the tup displacement reached a value that was equal to the sum of the specimen thickness and the diameter of the hemispheric nose. However, their impact testing was conducted under quasi-static loading rates (10-80 μm/s). They also observed a point where the load became a nearly constant value.

Based on the perforation points determined from the velocity-deflection curves, the absorbed energy values that matched the deflection values at perforation were used as the correct absorbed energies. This velocity-based method would abruptly end the load-deflection and velocity-deflection curves at the perforation points. The testing showed the loads gradually decreasing to zero after the friction portions of the load-deflection curves. The velocity-based method did not take into account this small area. This area only accounted for approximately 0.5 J of energy so it was deemed negligible.

B. Impact Energy

The impact energy, E_i, was based on the following equation

$$E_i = mgh + mgh' \qquad [6]$$

where m was the combined mass of the crosshead, load cell, and tup, g was the gravitational acceleration, h was the distance between the tip of the tup and the surface of the specimens before the drop tests took place and h' was the distance the tip travels from the moment of contact to the end of the impact event. The determination of h' was dependent on whether the tup rebounded or perforated the specimens. The maximum deflections calculated by Equation 6 were used if the tup rebounded from the specimens. The deflection values corresponding to the perforation points found from curves like those presented in Figure 6 were used if the tup perforated the specimens.

Extended Method

Besides the foregoing method used for obtaining correct impact energy and absorbed energy, an extended method was also investigated in attempts to determine the penetration threshold. This method was based on extending

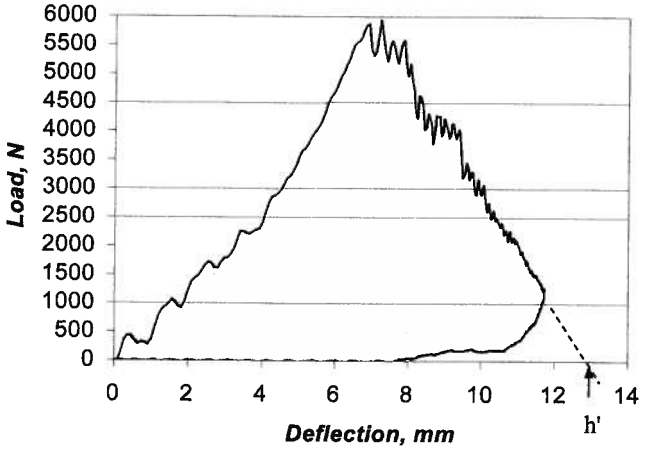

Figure 7a. Extended method for L[(0/90)$_6$] specimen 4.

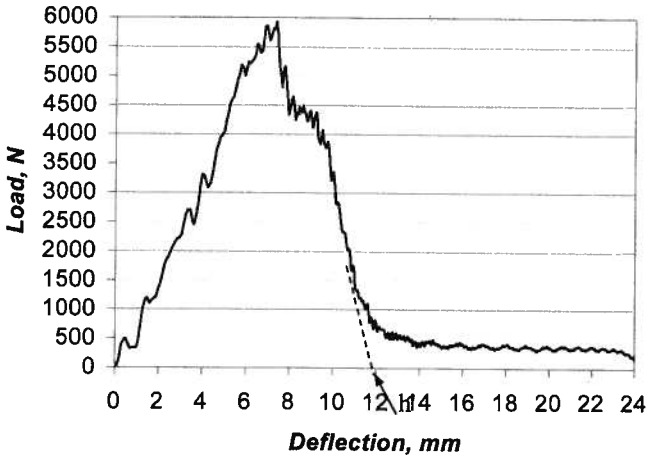

Figure 7b. Extended method for L[(0/90)^6] specimen 8.

the unloading section (excluding the rebouding part) to the deflection axis for both closed and open load-deflection curves. This method was used as an alternative way to estimate the amount of energy required for penetration as conducting an impact event right up to the point of penetration was almost impossible.

The load-deflection curve of the L[(0/90)$_6$] specimen 4 is presented in Figure 7a. The tup rebounded from this specimen as is evidenced by the curve being closed. This specimen could have absorbed more energy while being penetrated by the tup. The unloading section of the curve would have continued along its slope and intersected the deflection axis at a point beyond 12 mm if the tup had penetrated the specimen and not rebounded. This extension of the slope is shown by the dashed line. The post-perforation friction would not have occurred because the sides of the tup did not pass through the specimen. The extended load-deflection curve could be used to calculate the absorbed energy for penetration. The impact energy could also be calculated using Equation 6 where h' would be the deflection value at the intersection of the softening curve and the deflection axis as indicated in Figure 7a. Figure 7b illustrates how the extended method would be used for specimens that were perforated. The load recorded due to friction would not be exempted from calculating absorbed energy.

Table 1. Comparison of energies from different methods for L[(0/90)$_6$] specimens.

		Velocity-based Method			Extended Method		
specimen	tup	E_i (J)	E_a (J)	h' (mm)	E_i (J)	E_a (J)	h' (mm)
1	Rebounded	33.15	29.57	10.15	-	-	-
2	Rebounded	34.60	31.66	10.46	-	-	-
3	Rebounded	35.29	33.11	10.77	35.32	36.00	11.50
4	Rebounded	34.22	33.24	11.72	34.26	34.89	12.80
5	Rebounded	35.04	34.17	11.47	35.04	35.23	11.80
6	Perforated	35.06	33.90	11.43	35.07	34.14	11.80
7	Perforated	37.20	35.45	11.68	37.11	35.70	12.20
8	Perforated	40.77	36.85	12.45	40.73	36.10	11.80

This method would not work well if there was not a well defined unloading section of the load-deflection cureve. Specimens 1 and 2 of the L[$(0/90)_6$] plate could not be used for the extended method since they did not have well defined unloading sections. Table 1 presents the absorbed energies and impact energies of the L[$(0/90)_6$] specimens from the velocity based method and the extended method.

The velocity based method and the extended method produced similar results. The absorbed energies from the extended method for tests 3-5 are greater than those from the velocity based method because these tests had rebounding. The extended method shows how much energy may have been required to penetrate but not perforate the specimens for tests 3-5. The h' values from both methods were similar as shown in Table 1. The velocity based method had all absorbed energies less than the impact energies, while the extended method had absorbed energies slightly greater than impact energies for tests 3-5. These tests had rebounding sections so the absorbed energies are an estimate of how much they could have absorbed. Another possible explanation is that the extended unloading slope intercepted the deflection axis at a value greater than the truncated point determined by the velocity based method.

Experimental Results and Discussions

The velocity based method was chosen to present the energy data for all of the specimens tested. This method effectively eliminated the absorbed energy resulting from the sides of the tup and specimen interactions.

L[$(0/\theta)_6$] Plates

The load-deflection curves of the L[$(0/90)_6$] specimens is shown in Figure 5 and the associated absorbed energies are given in Table 1.The load-deflection curves of the specimens tested seem to overlap well in the loading and unloading sections, indicating consistency in both material properties and testing conditions. Specimens 2-6 were chosen to illustrate the penetration and perforation thresholds of the L[$(0/90)_6$] specimens. Specimens 2-5 were chosen because they were almost penetrated by the impact energy inputted to them. Specimen 6 was chosen because its value of impact energy just caused perforation. Specimen 1 experienced little damage and was not near to penetration so it was not used. Specimens 7 and 8 had severe perforation and were not used to characterize the specimens. The impact energy, E_i, and absorbed energy, E_a, of all L[$(0/\theta)_6$] specimens are given in Table 1. The range of absorbed energy for penetration and perforation was 31.66 J to 34.17 J. The differences between E_i and E_a for the chosen cases are below 3 J. These values indicate the minimum energy not absorbed by the specimens due to vibration and heat. The minimum difference was 0.86 J for the L[$(0/90)_6$] specimens.

All specimens produced similar mountain-shaped load-deflection curves when compared to the L[$(0/90)_6$] specimens. The same guidelines used in choosing L[$(0/90)_6$] plates for further analysis were used for all other composite plates. None of the specimens had absorbed energies exactly equal to their respective impact energies. Experimental results revealed that a minimum amount of energy about 1 J seemed to be lost in the tests due to vibration and heat for all tests. The energies produced from the tests were not able to determine the exact penetration and perforation because none of the samples had a large impact energy interval between penetration and perforation. This was likely due to the specimens being very thin. In other words, there was no remaining material for the tup to penetrate into once it made initial penetration. The testing results did reveal a small range of impact energies for each type of composite plates where the tup would almost penetrate or just perforation. This range of impact energies seemed to be useful for characterizing the impact resistance of the composite plate.

Effect of Small Fiber Angle

The testing results revealed that fiber orientation had a remarkable influence on impact resistance. Figure 8 shows that the impact resistance for laminated specimens increased as the fiber angle, θ, was decreased. The bending stiffness mismatch [x] in the specimens was believed to be responsible for this result. The bending stiffness mismatch was dependent on the difference of fiber orientation between adjacent laminas. It increased as the difference of fiber orientations was increased. This bending stiffness mismatch caused the

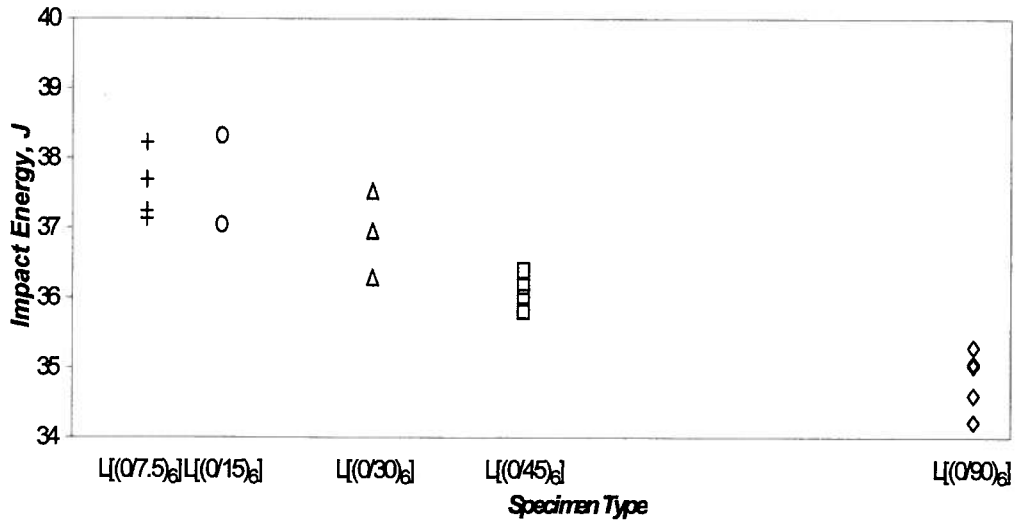

Figure 8. Impact energy interval of laminated specimens.

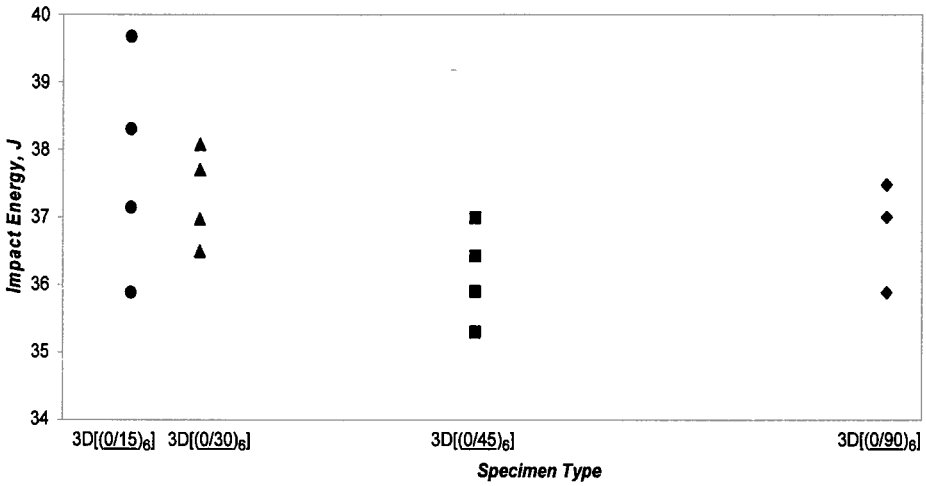

Figure 9. Impact energy interval of 3D specimens.

composite specimens to delaminate when the interlaminar stress was higher than the allowable levels. Once delamination formed, the tup could perforate the delaminated specimens easier than specimens that were not delaminated[5,17,19]. The results of Figure 8 seemed to support this viewpoint. Small values of θ caused the specimens to delaminate less, hence increasing the impact resistance. The $L[(0/90)_6]$ specimens had the largest bending stiffness mismatch causing the largest delamination, thus the lowest impact resistance. On the contrary, the $L[(0/7.5)_6]$ and $L[(0/15)_6]$ specimens had smaller bending stiffness mismatch causing less delamination, thus larger impact resistance.

The results of the 3D woven specimens given in Figure 9 show a similar dependence on fiber orientation except for a small discrepancy in the $3D[(\underline{0/90})_6]$ specimens. The load-deflection curves of the $3D[(\underline{0/90})_6]$ were not as consistent as other cases and that might be responsible for the discrepancy.

Effect of 2D and 3D Weaving

The specimens tested have had varying degrees of through-thickness reinforcement. The laminated specimens had no through-thickness reinforcement. The only material joining the adjacent plies was the thin layer of matrix between them. There were no fibers contributing to any through-thickness strength.

The stitched specimens and the laminated specimens were similar in that they were both initially $L[(0/90)_6]$ specimens. The stitched specimen used 1 mm wide strips of prepreg as stitching thread to join the plies together besides the thin layer of matrix. Stitching through the thickness with a 12.5 mm x 12.5 mm square pattern proved to be the best through-thickness reinforcement method, among the composites tested, as shown in Figure 10. It was likely that this stitching pattern and density were an efficient selection. A stitching pattern with a higher density may not have been efficient enough. On the other hand, a stitching pattern with a lower density may have caused higher stress concentrations.

Each piece of the 2D woven specimens consisted of two plies that were interwoven. This interweaving reinforced each piece through the thickness. Six pieces were then stacked together to form the completed 2D woven specimens. As a result, the 2D woven specimens had more through-thickness reinforcement than the laminated specimens. This caused the 2D woven specimens to require slightly higher energy to begin penetration and perforation than the laminated specimens.

The 3D woven specimens were reinforced through the thickness by fibers although they were not oriented in the thickness direction. This made them more resistant to penetration and perforation when compared to the 2D woven and laminated specimens.

The 3D woven plates were fabricated with four different θ values that were 15°, 30°, 45°, and 90°. Four of the laminated plates shared the same θ values. The 3D woven specimens had larger energy intervals than the laminated specimens. This was the most obvious when looking at the results of the $3D[(0/15)_6]$ specimens. The $3D[(0/30)_6]$ specimens performed slightly better than $L[(0/30)_6]$ specimens. The testing results showed less impact energy was required to begin perforation in the $3D[(0/45)_6]$ specimens when compared to the $L[(0/45)_6]$ specimens. The energy interval for the $3D[(0/45)_6]$ specimens was larger while the energy to cause perforation was greater. The $3D[(0/90)_6]$ specimens showed the largest improvement on impact resistance when compared to the $L[(0/90)_6]$ specimens.

Effect of Delamination

Visual inspections showed a decrease in delamination area in the 3D woven specimens, which seemed to not propagate as far from the impacted area as in the laminated specimens. Figure 11 compares $L[(0/45)_6]$ speci-

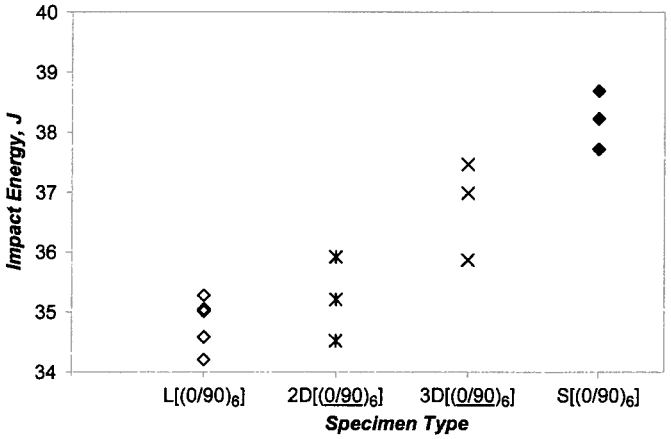

Figure 10. Impact energy interval of $[(0/90)_6]$ specimens.

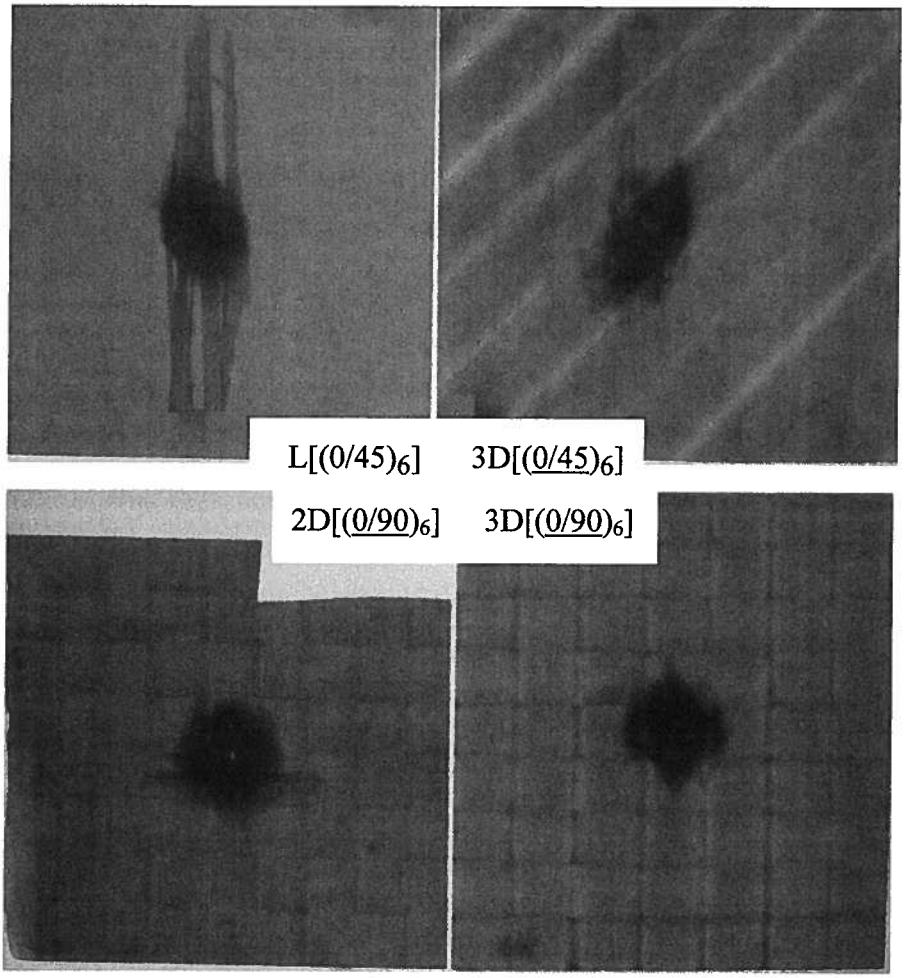

Figure 11. Damaged composite specimens.

men 5 to 3D[(0/45)$_6$] specimen 6. They were subjected to impact energies of 36.39 J and 36.42 J, respectively. Delamination is shown by the darker areas of the specimens when the specimens are placed on a light table and photographed. The laminated specimen delaminated more than the 3D woven specimen. The delamination of the bottom ply extends almost the entire length of the specimen. The 3D woven specimen delamination seemed to pass slightly beyond the undulations of the warp and fill strips. The undulation and interweaving of the strips (tows) in the 3D woven specimens seem to constrain the delamination growth.

The delamination of 2D[(0/90)$_6$] specimen 1 and 3D[(0/90)$_6$] specimen 1 is compared in Figure 11. The specimens were impacted with energies of 34.53 J and 34.57 J, respectively. The delamination area of the 2D woven specimen was larger than the 3D woven specimen. The 2D woven specimen had delamination extend away from the impact point. The 3D woven specimen seems to contain the delamination to an area close to the point of impact, i.e. at the center of the unit cell.

Effect of Stitching

The through-thickness reinforcing mechanism in the stitched specimens was different from that of woven ones. Instead of confining the delamination to the dimensions approximately equal to a unit cell as in the woven specimens, stitched specimens provided through-thickness reinforcement through the tensile strength of the stitching threads. As shown in Figure 12, some stitching threads were stretched to fracture by the impact tup. Hence, the impact resistance should be increased with the tensile strength of broken threads. It then was expected that the location and size of the threads should have noticeable effect on the impact resistance. In fact, the study was based on an "optimal condition" in that that all 2D woven, 3D woven and stitched specimens were impacted particularly at the center of the cell, resulting in more optimal results. Therefore, the order of the impact resistance should not be overlook while the fact of the through-thickness reinforcement should be trusted.

Conclusions

Composite plates made from glass/epoxy prepreg tapes were laminated, stitched, and woven with conventional two-dimensional and innovative three-dimensional fabric geometries. Laminated specimens L[(0/θ)$_6$] constructed with θ angles of 7.5° and 15° had higher impact resistance than specimens with θ angles of 30°, 45° and 90°. These results were consistent with the results that 3D[(0/15)$_6$] and 3D[(0/30)$_6$] had higher impact resistance than 3D[(0/45)$_6$] and

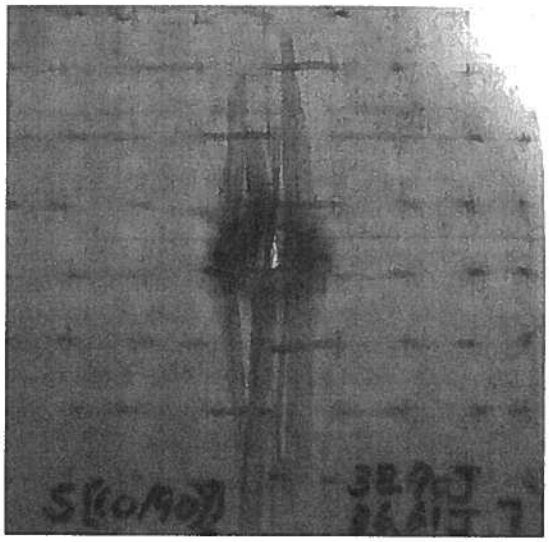

Figure 12. Damaged S[(0/90)$_6$] specimens.

3D[(0/90)$_6$]. It was then concluded that through-thickness smaller fiber angles between adjacent layers gave higher impact resistance. In terms of through-thickness fiber geometry, the stitched specimens had the highest impact resistance followed by the 3D woven specimens which outperformed the 2D woven specimens. The laminated specimens had the lowest impact resistance. Results from both studies seemed to point out the strong correlation between the high impact resistance and high delamination resistance.

Acknowledgements

The authors wish to express their sincere thanks to the U.S. Army RDECOM/TARDEC for financial support.

References

1. J. Jovicic, A. Zavaliangos, F. Ko, "Modeling of the Ballistic Behavior of Gradient Design Composite Armors," *Composites Part A*, Vol. 31, 1996, pp. 773-784.

2. J.K.Kim, M.L. Sham, "Impact and Delamination Failure of Woven-Fabric Composites," *Composites Science and Technology*, Vol. 60, 2000, pp. 745-761.

3. G. Davies, D. Hitchings, G. Zhou, "Impact Damage and Residual Strengths of Woven Fabric Glass/Polyester Laminates," *Composites Part A*, Vol. 27, 1996, pp. 1147-1156.

4. L. Sutherland, C. Soares, "Effects of Laminate Thickness and Reinforcement Type on the Impact Behavior of E-Glass/Polyester Laminates," *Composites Science and Technology*, Vol. 59, 1999, pp. 2243-2260.

5. D. Liu, "Delamination Resistance in Stitched and Unstitched Composite Plates Subjected to Impact Loading," *Journal of Reinforced Plastics and Composites*, Vol. 9, 1990, pp. 59-69.

6. M.O.W.Richardson, M.J. Wisheart, "Review of Low-Velocity Impact Properties of Composite Materials," *Composites Part A*, Vol. 27A, 1996, pp. 1123-1131.

7. G. Davies, D. Hitchings, J. Wang, "Prediction of Threshold Impact Energy for Onset of Delamination in Quasi-Isotropic Carbon/Epoxy Composite Laminates Under Low-Velocity Impact," *Composites Science and Technology*, Vol. 60, 2000, pp. 1-7.

8. N.K. Naik, S. Meduri, "Polymer-Matrix Composites Subjected to Low-Velocity Impact: Effect of Laminate Configuration," *Composites Science and Technology*, Vol. 61, 2001, pp. 1429-1436.

9. L.C. Dickinson, G.L. Farley, M.K. Hinders, "Translaminar Reinforced Composites: A Review," *Journal of Composites Technology and Research*, Vol. 21, No. 1, 1999, pp. 1178-1202.

10. F. Larsson, "Damage Tolerance of a Stitched Carbon/Epoxy Laminate," *Composites Part A*, Vol. 28A, 1997, pp. 923-934.

11. A.P. Mouritz, "Flexural Properties of Stitched GRP Laminates," *Composites Part A*, Vol. 27, 1996, pp. 525-530.

12. A.P. Mouritz, M.K. Bannister, P.J. Falzon, K.H. Leong, "Review of Applications for Advanced Three-Dimensional Fibre Textile Composites," *Composites Part A*, Vol. 30, 1999, pp. 1445-1461.

13. L. Walker, M.S. Sohn, X.Z. Hu, "Improving Impact Resistance of Carbon-Fibre Composites Through Interlaminar Reinforcement," *Composites Part A*, Vol. 33, 2002, pp. 893-902.

14. N.K. Naik, S.V. Borade, H. Arya, M. Sailendra, S.V. Prabhu, "Experimental Studies on Impact Behavior of Woven Fabric Composites: Effect of Impact Parameters," *Journal of Reinforced Plastics and Composites*, Vol. 21, No. 15, 2002, pp. 1362.

15. T. Ebeling, A. Hiltner, E. Baer, I.M. Fraser, M.L. Orton, "Delamination Failure of a Woven Glass Fiber Composite," *Journal of Composite Materials*, Vol. 31, No. 13, 1997, pp. 1318-1333.

16. Y.P. Siow, V.P.W. Shim, "An Experimental Study of Low Velocity Impact Damage in Woven Fiber Composites," *Journal of Composite Materials*, Vol. 32, No. 12, 1998, pp. 1178-1202.

17. D. Liu, B.B. Raju, X. Dang, "Impact Perforation Resistance of Laminated and Assembled Composite Plates," *International Journal of Impact Engineering*, Vol. 24, 2000, pp. 733-746.

18. J.N. Baucom, M.A. Zikry, "Evolution of Failure Mechanisms in 2D and 3D Woven Composite Systems Under Quasi-Static Perforation," *Journal of Composite Materials*, Vol. 37, No. 18, 2003, pp. 1651-1674.

19. D. Liu, "Impact Induced Delamination – A View of Bending Stiffness Mismatching," *Journal of Composite Materials*, Vol. 22, 1988, pp. 674-692.